Appendix H—Maximum Likelihood Recurrence Intervals for California Paleoseismic Sites

By Glenn P. Biasi[1]

Summary

This appendix provides estimates of long-term mean recurrence intervals and rates and their respective uncertainties for 32 paleoseismic sites on California faults. The Uniform California Earthquake Rupture Forecast, Version 3 (UCERF3) Grand Inversion (appendix N, this report) uses these estimates as one constraint among many to solve for the rates of fault ruptures in California. Maximum likelihood (ML) methods are applied to the paleoseismic event dates to estimate parameters and uncertainties for the log-normal and exponential recurrence distribution models. Open intervals since the most recent event are used where available. We show in synthetic tests that ML parameters are not systematically biased even for short paleoseismic records. Two approaches were used to develop long-term mean recurrence intervals. The exponential model provides one direct estimate in the calculation of its rate parameter. Another long-term mean can be calculated from the log-normal mean and variance parameters. These estimates will converge for very long series, but with limited data they can differ, primarily because log-normal estimates are less sensitive to the length of the open interval. A degree of time dependence is observed in most long paleoseismic series in California. Also, modified Akaike Information Criteria (AICc) generally favor the log-normal model where the AICc resolves between models. Therefore the long-term mean rates are estimated using the ML log-normal parameter sets. A few event series are too short to provide log-normal parameters; for these cases, exponential rate estimates are provided. Resulting long-term mean rates and 2.5-, 16-, 84-, and 97.5-percent uncertainties are provided as inputs for the Grand Inversion. A likelihood surface approach is presented to show the relationship among equally likely model parameter pairs. The likelihood surface for the South Hayward site shows that a previous estimate of 210 years should now be considered improbable. New estimates may also be compared to those from UCERF2. The UCERF2 estimates vary, significantly in many cases, around the current ML values.

Introduction

Earthquake recurrence at paleoseismic sites provides a fundamental, data-derived estimate of long-term seismic hazard on faults. Catalogs of seismic data do not cover long enough time periods to provide these estimates, and seismicity rates on many important faults are known to underpredict fault behavior at large magnitudes. For these reasons paleoseismic earthquake recurrence is an important contributor in long-term regional hazard estimates.

[1]University of Nevada, Reno.

The occurrence of ground rupture at sites along active faults is established by paleoseismologists by the application of geologic, structural, and chronologic methods to trench-scale deformations and discontinuities. Normally paleoseismic ground ruptures are not dated directly, but rather are bounded by youngest radiocarbon dates of disrupted layers and the oldest samples from an overlying undisrupted layer. Layer dates can be improved by applying stratigraphic ordering information (Biasi and Weldon, 1994; Lienkaemper and others, 2010), but rarely are better defined than a few decades. Ruptures dated by bounding inherit uncertainties from the layer dates. In California, a few event dates of large events are known from historical accounts, including the San Andreas events of 1812, 1857, and 1906, and the Hayward fault event of 1868. In general, paleoseismic-event series for California sites consist of a mixture of precise historical and uncertain paleoseismic dates.

The objectives of this appendix are threefold:

- Present and describe a maximum likelihood (ML) process for estimating recurrence interval (RI) parameters from paleoseismic event series.
- Develop ML parameter estimates for log-normal and exponential distributions for UCERF3 paleoseismic sites.
- Provide mean recurrence interval and rate estimates and respective 2.5-, 16-, 84-, and 97.5-percent uncertainties

Data Basis for UCERF3 Recurrence Interval Estimation

The primary data source for recurrence interval parameter estimation is UCERF3 appendix G (this study). Sites with three or more events or two events and an open interval were analyzed. Probability density functions (PDFs) for earthquake dates were available or could be developed for some sites. For the south Hayward site, the OxCal model of Lienkaemper and others (2010) was rerun and event PDFs were extracted from the OxCal output (Lienkaemper and Bronk-Ramsey, 2009). PDFs generated by the author were used for the Wrightwood (Biasi and others, 2002) and most recent Pallett Creek (Scharer and others, 2011) records. Where appendix G (this study) gives only central 95-percent date ranges, date PDFs were synthesized using a Gaussian shape applied symmetrically to these ranges. Note that this allows event dates outside the ranges of appendix G (this study) at commensurably small probabilities. Examples of the two types of event chronologies are shown in figure H1. Other notes on the data sources are provided in table H1.

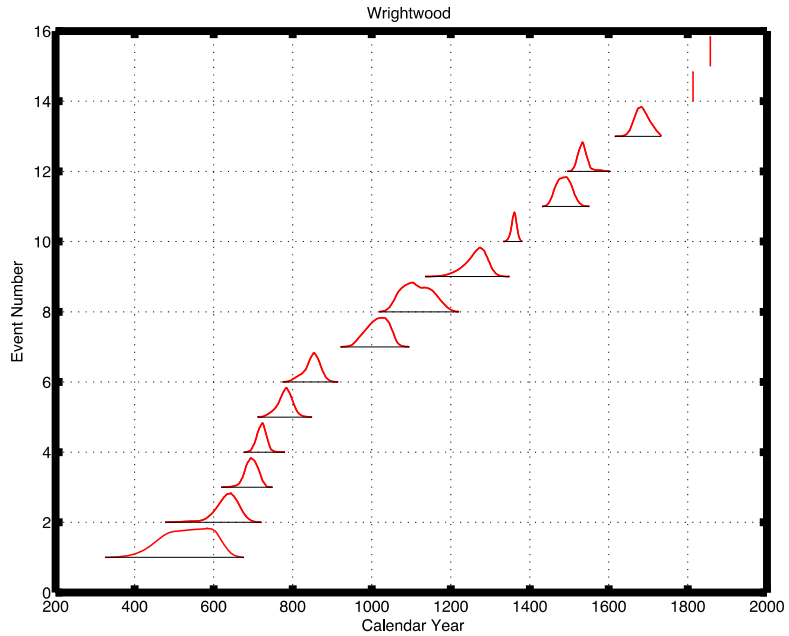

(A)

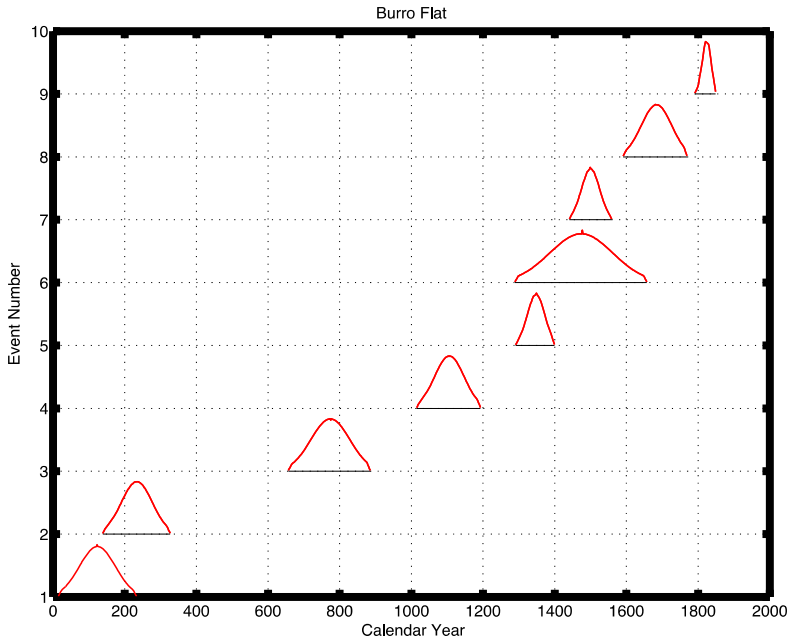

(B)

Figure H1. Earthquake date probablility distribution functions (PDFs) for two sites used as inputs for parameter estimation. Event numbers are given on the vertical axis. *A*, Wrightwood upper section with PDFs from Bayesian analysis (Biasi and others, 2002). Vertical bars are historic 1812 and 1857 events. *B*, Burro Flat. For these events, only a date range was available, so the date structure was added as a Gaussian distribution. Though these are Gaussian, note that they are not identically distributed. Event number 9 is the historical 1812 event. All event PDFs have been normalized for plotting purposes to the same height.

Table H1. Site-by-site review of data used to calculate maximum likelihood recurrence intervals for California faults.

[Nev, number of events; MRE, most recent event; PDF, probability distribution function; UCERF3, Uniform California Earthquake Rupture Forecast, version 3; PE, penultimate event; RI, recurrence interval; SAF, San Andreas Fault; N. SAF, northern San Andreas Fault; S. SAF, southern San Andreas Fault]

Fault and site	Nev	Closed total time (yrs)	Time since MRE* (yrs)	Adjustments relative to UCERF3 appendix A (this study); UCERF3 appendix G (this study); and other notes
Calaveras North	4	1382	720	Prehistoric MRE
Compton	6	11,105	1208	Prehistoric MRE
Elsinore – Glen Ivy	6	872	102	MRE in 1910
Elsinore – Julian	2	1502	1750	Notes indicate record may be incomplete. Pre-historic MRE
Elsinore – Temecula New	3	1996	N/A	Left censor information for oldest event was not used; youngest event is not the site MRE
Elsinore-Whittier	2	1407	1791	Prehistoric MRE
Garlock Central	6	6378	470	Prehistoric MRE
Garlock West	5	4716	326	Dates from Madden-Madugo and others (2012). Event 6 considered equivocal by them and not included here. Prehistoric MRE
Green Valley—Mason	4	602	411	Prehistoric MRE
North Hayward (Mira Vista)	8	2003	301	Prehistoric MRE
South Hayward, Tyson Lagoon	12	1777	145	Event PDFs calculated from Lienkaemper and others' (2010) OxCal model. Historic MRE in1868
Little Salmon (Strong's Creek)	3	2650	10,840	Prehistoric MRE; time since MRE>>apparent RI of events; record potentially incomplete; not used in the UCERF3 Grand Inversion (appendix N, this study)
N. SAF Alder Creek	2	784	107	Historic MRE in 1906.
N. SAF Santa Cruz Segment	10	847	107	Hybrid to represent the Santa Cruz segment of the SAF. Events consist of the Arano Flat record with two changes: Arano PE = historic 1890, and the former Arano E2 was redated to historic 1838. MRE in 1906. UCERF3 uses this in lieu of Arano Flat, Mill Canyon, and Hazel Dell
N. SAF Fort Ross	4	923	107	Historic MRE in 1906
N. SAF Vedanta N. Coast	12	2732	107	Historic MRE in 1906
N. SAF Noyo	15	2548	107	Events assigned ±100 year uncertainties; event mean dates calculated from preferred interval lengths working backward from 1906 MRE
Puente Hills	3	7122	249	Prehistoric MRE
San Gregorio North	2	528	487	Prehistoric MRE
Rodgers Creek	3	452	303	Prehistoric MRE
San Jacinto – Hog Lake	14	3235	243	Prehistoric MRE
San Jacinto – Superstition Mountain	3	508	462	Prehistoric MRE
S. SAF Bidart (Carrizo)	6		156	Historic MRE in 1857.
S. SAF Burro Flat	7	1039	201	Historic MRE in 1812.
S. SAF Coachella	7	753	320	Nev=7 adopted for consistency with Parsons (2013); prehistoric MRE circa 1690
S. SAF Frazier	8	830	156	Historic MRE in 1857

Fault and site	Nev	Closed total time (yrs)	Time since MRE* (yrs)	Adjustments relative to UCERF3 appendix A (this study); UCERF3 appendix G (this study); and other notes
Mountain				
S. SAF Indio	4	659	334	Prehistoric MRE circa 1690
S. SAF Pallett Creek	10	1213	156	Event C added from Biasi and others (2002). Historic MRE in 1857
S. SAF Pitman Canyon	7	887	201	Pit2 with a paleoseismic uncertainty and mean calendar date of 1704 was adopted as the PE. Historic MRE, 1812
S. SAF Plunge Creek	3	350	201	Historic MRE in 1812
S. SAF Thousand Palms	5	858	331	Prehistoric MRE circa 1690
S. SAF Wrightwood	15	1333	156	Event PDFs from Biasi and others (2002); includes event T extrapolated from Pallett Creek (Weldon and others, 2004). Historic MRE in 1857

*Time since prehistoric MRE is 2013 minus the mean sampled date of the MRE.

Estimates in this appendix address the temporal recurrence of ground rupturing displacements at individual locations. We regard as given that the reported observations are accurate in their essential qualities including identification of the rupture evidence, association of the evidence with an earthquake cause, and association of the evidence with relevant absolute dates. Displacements and indicators of relative event size are not used. Weldon and others (appendix G, this report) review the paleoseismic data and displacement evidence available to UCERF3, and their results have been adopted directly.

Recurrence Interval Parameter Estimation Methods

Many methods for recurrence interval parameter estimation have been presented in the paleoseismic literature. Standard methods for common recurrence models are well known from statistics texts. Uncertainty in the paleoseismic event dates presents complications for parameter estimation. Ellsworth and others (1999) sampled from the event dates and used a bootstrap method to estimate uncertainties. Biasi and others (2002) use the event dating uncertainty directly. They draw thousands of samples of size N from event dates (where N is the number of events at the site), and use maximum likelihood methods to find log-normal and exponential distribution parameters for the Wrightwood and Pallett Creek paleoseismic sites on the southern San Andreas Fault (SAF). They did not formally include the open interval, reasoning that it was similar in length to the site mean and that it would have little effect on the estimates. Parsons (2008a) estimated recurrence parameters using a variant of the Maximum Likelihood method. These estimates were developed for UCERF2, but the method was ineffective for modeling long series and series with precisely known (that is, historical) intervals. As a result, parameter estimates using the Biasi and others (2002) method were developed for UCERF2 Type A faults (Dawson and others, 2008). For other perspectives and methods, consult Bakun and Lindh (1984), Cornell and Winterstein (1988), Savage (1993), Sykes and Menke (2006), and Parsons (2012).

Maximum Likelihood Parameter Estimation

Paleoseismic event series are inevitably a sample of small size drawn from a physical system that creates ground rupture and presumably significant earthquakes. A basic distinction must be preserved between variability in an observed paleoseismic event series and variability in the underlying process. The statistical parameters of the physical system (the population statistics) are unknown, but presumably sufficiently stationary that the past can be used to infer statistics for the next event. Given some limited sample of earthquake intervals and their uncertainties, the main challenge in earthquake-recurrence-rate estimation is understanding the true underlying rate and its uncertainties.

A principle of recurrence interval estimation methods is that they should work without modification of any mixture of historical and uncertain dates. Historical events are an end member for hazard estimation purposes because the time of the event is known to within a small fraction of the interseismic interval (that is, a day or less). A sequence comprised entirely of historical events would provide the most precise sample of data about earthquake recurrence at that site, but the intrinsic uncertainty associated with sampling from a random process remains. For example, while the mean and variance of a given sample might be known with some precision, the sampling contribution to recurrence interval uncertainty may be (and often is) disconcertingly large. The focus of maximum likelihood estimation procedures is to identify the most likely underlying process parameters given the (fuzzy) data that we have.

Maximum likelihood methods were introduced by R.A. Fisher (1922). The ML method uses something of an inverse approach: Given the data and a distribution model, what is the best estimate and likely range of parameters that may have given rise to these data? A noteworthy property of the ML approach is its strict basis in observations. On the one hand this may not seem wise, because, for example, a short-time-interval sample is unlikely to observe the full behavior of the system, especially for an underlying distribution with a long tail. On the other hand, asserting information from sources other than the data itself implies knowledge about the real system that is not expressed in the sample, or equally, knowledge of what is missing from the sample. We explore this topic further in a later section.

We develop recurrence-interval-parameter estimates for two model distributions. For paleoseismic sites with two or more intervals, parameters are developed using the log-normal distribution,

$$f(t \mid \mu\sigma) = \frac{1}{t\sigma\sqrt{2\pi}} \exp\left(\frac{-(\ln t - \mu)^2}{2\sigma^2} \right) \qquad (1)$$

It models the natural logs of recurrence intervals as being normally distributed around mean μ with variance σ^2. The symmetry in log space means that in the time-domain, intervals twice the average length and half the average length are equally likely. Because the log-normal distribution is defined only for positive intervals, its distribution is asymmetric, with a potentially significant right tail (fig. H2). Physically, the log-normal distribution corresponds to a case where factors affecting recurrence combine as products of one another. The sample mean μ_{ln} of the logs of observed RIs is the minimum variance unbiased estimator for μ (for example, Larson, 1982). Unbiased means that the sample mean converges to the population mean as the sample size increases. Minimum variance means that the sample mean is associated with the narrowest range

of uncertainties among possible unbiased estimators of μ. Other estimates might be proposed (for example, the median), but the ML properties are well researched and suited to the present needs.

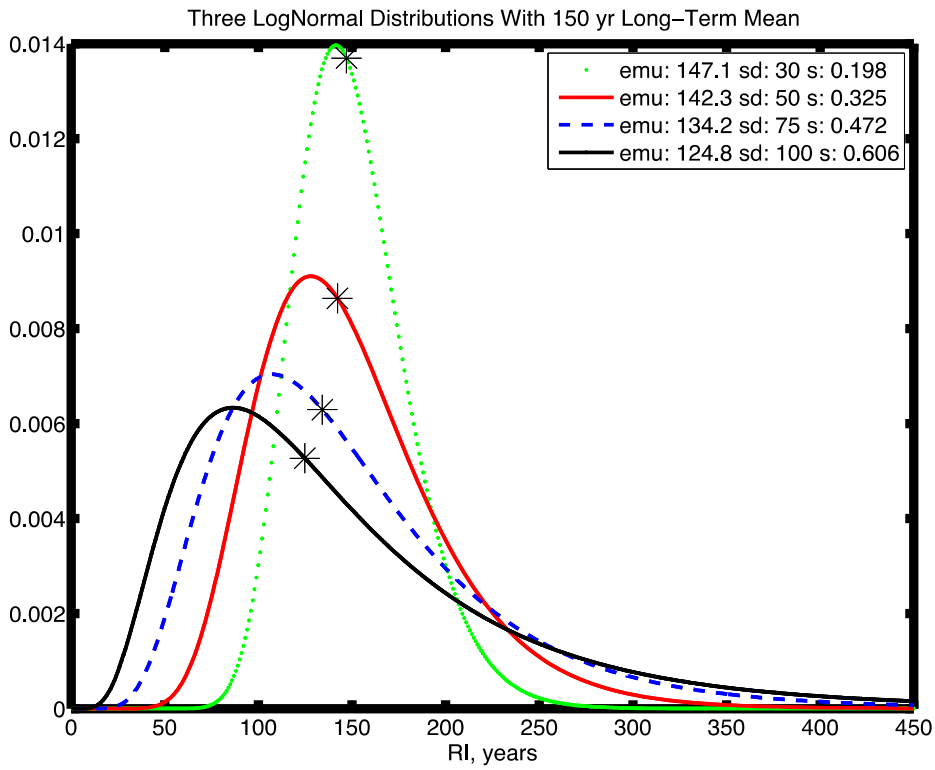

Figure H2. Four log-normal distributions all having the same 150-year long-term mean. Width of standard deviation (sd), in years, corresponds with log-standard deviation (s=σ). Black stars mark emu=exp(μ) values, which are a function of variance for a given long-term mean rate.

While the ML estimate μ_{ln} from the sample mean is an unbiased estimator of the underlying log-normal location parameter, it is not the mean long-term event-recurrence rate. The long-term mean rate is equal to the expected value of the ML distribution:

$$E(t \mid \mu_{\ln}, \sigma_{\ln}) = \int_0^\infty t f(t \mid \mu_{\ln}, \sigma_{\ln}) dt \qquad (2)$$

which for the log-normal distribution yields:

$$E(t|\mu_{\ln}, \sigma_{\ln}) = \exp(\mu_{\ln} + \sigma_{\ln}^2/2) \qquad (3)$$

As equation 3 makes clear, E(t) is systematically larger than an interval estimate from $\exp(\mu_{ln})$ alone, with the difference being a function of the variance. Figure H2 considers equation 3 another way, with four examples, all with the same expected value of 150 years, but with a range of time uncertainties on the RI from thirty to one hundred years. Parameters μ_{ln} and σ_{ln} compensate in opposite ways to keep the expected value fixed. Increasing the variance gives

more weight to rare long intervals, and mean log point μ_{ln} adjusts to the left and increases the probability of shorter intervals to maintain a balance at the expected value (the long-term mean). As an aside, the mode $M(\mu_{ln}, \sigma_{ln}) = \mu_{ln} - \sigma_{ln}^2/2$ is the maximum point of the continuous distribution and is as far below the ML estimate of μ_{ln} in log space as the expected value (long-term mean) is above it.

Estimates of recurrence-interval parameters are also estimated using the exponential distribution, which is a single-parameter model where the ML estimate is the sample mean, and variance is equal to the mean. The exponential distribution,

$$f(x|\lambda) = \lambda e^{-\lambda x} \tag{4}$$

characterizes the time between events that can be described as random in time (that is, Poisson). The exponential-model parameter estimate λ_e is the only parameter that can be offered when the data consist of one interval and a censored period since the most recent event (MRE). The uncertainties in samples with one or two intervals are generally so large that the data offer very little constraint on recurrence.

Ellsworth and others (1999) and Matthews and others (2002) proposed another distribution for recurrence intervals known as the Brownian Passage Time (BPT) model. Like the log-normal, the BPT model can also be expressed with two parameters, in this case a mean and a coefficient of variation. BPT models recurrence as the first exceedence time of a combination of a linear term that monotonically increases in time with a periodically applied Gaussian step as in conventional Brownian motion. The linear term might correspond to a constantly increasing tectonic load and the random term to the influence of variations in background stress, earthquake interactions, or fault properties. The BPT also has a long right tail for fits to typical recurrence interval data. Available data are insufficient to distinguish between the BPT and log-normal distributions based on their numerical likelihoods (Biasi and Scharer, 2012). An argument in favor of the BPT has been made on the basis of its nonzero asymptotic hazard function (Matthews and others, 2002). However, for timeframes and requirements of UCERF3 forecasting, this property is of little practical advantage.

Potential Bias in ML Estimates of Recurrence

As noted earlier, longer-than-average intervals could be missing in a short paleoseismic record. This potential omission has been suggested to explain some longer-than-expected recurrence-interval estimates (for example, Parsons, 2008a). The potential for missing long intervals has also been cited in support of an alternate strategy in which recurrence parameters are estimated from the data distribution folded around its mean, and using the mode to characterize the log distribution (Parsons, 2012).

Synthetic test cases were developed to explore the nature and extent of potential bias in ML log-normal RI parameter estimates (fig. H3). As a first test (fig. H4), 1,000 records of some number of intervals (sample size from two to ten) were generated using a log-normal random number generator (150-year long-term mean, 30- and 70-year equivalent σ_{ln} cases) and then fit using the log-normal parameter estimation tool in the Matlab software package. Figure H4 shows the distribution of long-term mean estimates. Focusing on the mean of many trials, results show that if the paleoseismic record consists of at least three events and two intervals, the closed period from the first event to the last recovers, on average, an unbiased estimate of the long-term mean. Shorter series have a greater spread in potential μ_{ln} estimates, as would be expected.

Focusing on the spread of estimates, figure H4 can be interpreted to show the range of estimates one might find among individual samples despite having the same underlying long-term rate. This range increases with σ_{ln}. We conclude that the input mean is recovered without bias by the ML fitting procedure.

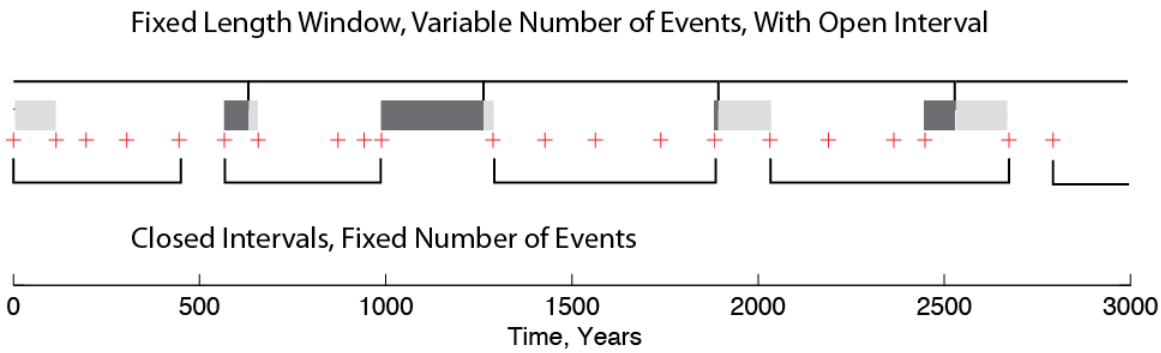

Figure H3. Two models used to test for bias in ML parameter estimates. Red "+" symbols are interval end points, starting at 0, generated at random with a 150-year long-term mean and σ corresponding to 70 years. Lower brackets opening upward indicate closed time windows with variable length (here, 450 yr) but having equal numbers of events. Upper, fixed width time windows (for variety, windows of 650 yr) have variable numbers of events in them, with open intervals at both ends. The dark gray line is the time since the most recent event, and is used to estimate maximum likelihood parameters. The open interval (light gray) after the window starts but before the first event is not included in the maximum likelihood estimation. Window lengths as short as three times that of the long-term mean show no material bias in their average estimates.

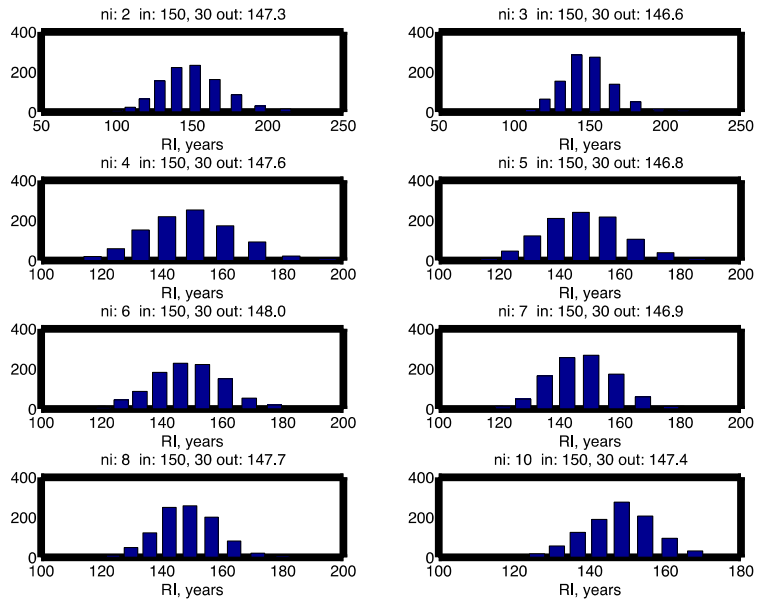

(A)

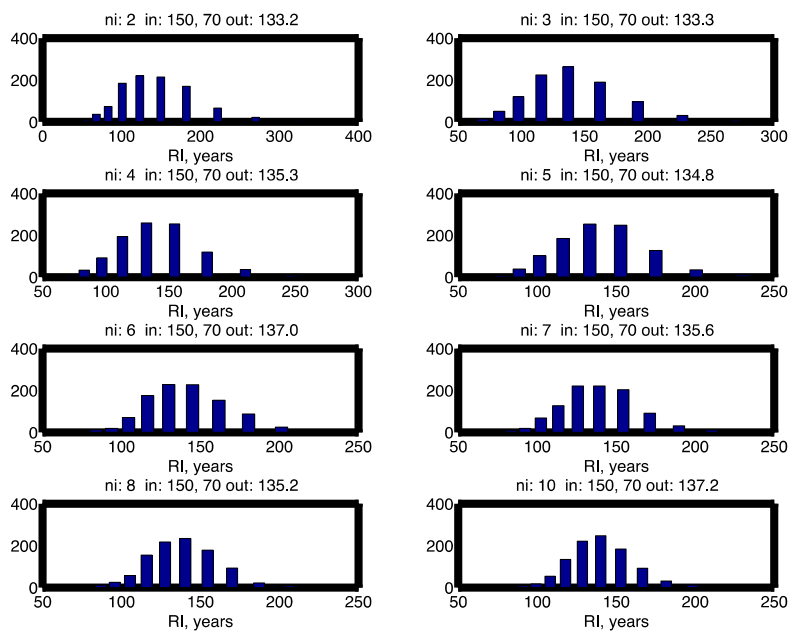

(B)

Figure H4. Histograms of parameter exp(μ_{ln}) for 1,000 trials using samples of size ni=2 to 10 recurrence intervals (RIs), drawn as log-normal random variables. *A*, Long-term mean RI=150, σ_{ln}=0.198 (30 years), exp(μ_{ln})=147.1 years. Recovered values for exp(μ_{ln}) are in the titles and are uniformly good approximations of the input. *B*, Mean RI=150, σ_{ln}=0.444 (70 years), exp(μ_{ln})=135.9 years. When a closed interval bounded by events defines the record length, the input mean parameter μ_{ln} is recovered with as few as three events and two intervals. Uncertainty decreases as the sample size increases.

Figure H5 shows a test more representative of the paleoseismic data. The input series consists of 5,000 log-normal intervals using a long-term mean of 150 years and an equivalent variance of 50^2 years (μ_{ln}=142.3 yr). A comb of windows of a fixed width is dropped on the series, and whatever events are inside each window are then fit as a sample for log-normal parameters (fig. H3). Thus the number of intervals and the length of time from the first event to the last varies from one window to the next. Unlike figure H4, the open interval since the most recent event is also included as censored data. The time since the MRE is measured from the latest event in the series to the right edge of the window. The distribution of left- and right-censored intervals is show in figure H6. Because only the minimum length of the final interval is known, the ML estimate is developed by an inverse process that solves for the most likely log-normal parameters that explain both the definite data and the open time since the MRE. Figure H5 shows the distribution of input right-censored interval lengths included in the fitting. The open interval tends to increase the estimate of μ_{ln} by slightly down-weighting the probability of shorter intervals. However, even for event series as short as three intervals the average increase of the mean μ_{ln} for this sample set is about two percent (145.6 versus 142.3 years). Even this modest increase is not properly interpreted as a bias because the open interval is positive evidence in the observed data favoring a slightly larger μ_{ln} estimate. Thus we find no evidence that short paleoseismic record lengths should be prone to missing longer intervals in any way that would systematically affect recurrence-interval parameter estimation.

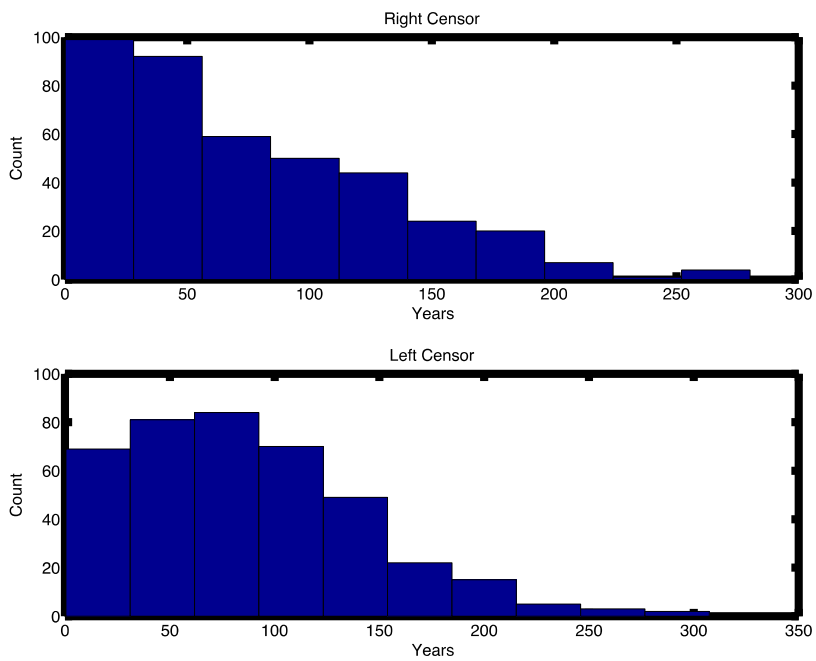

Figure H5. Histogram of right and left censored interval lengths for the random log-normal series used in Figure H5. The input mean=150 years, μ_{ln}=142.3 years, σ_{ln}=50 years. The right censor information (upper graph) carries the information about the time since the most recent event.

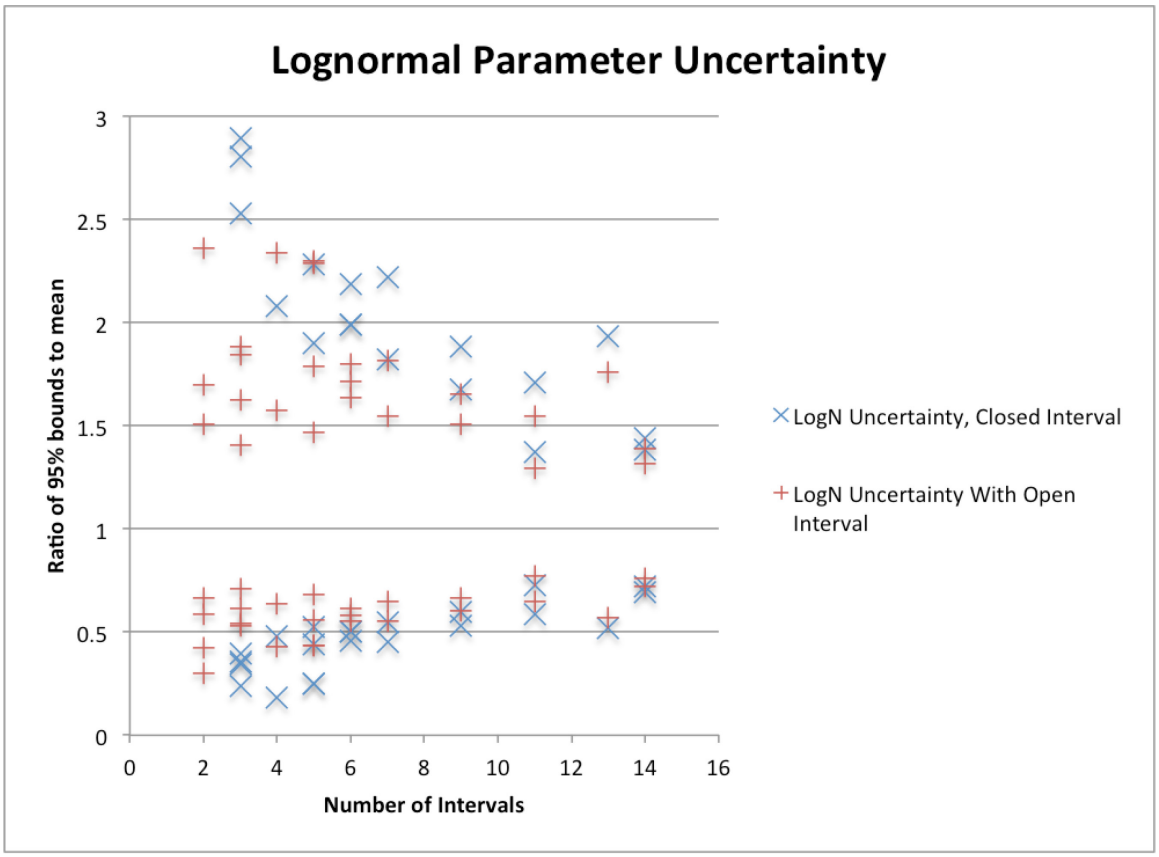

Figure H6. Plot showing the range in log-normal mean parameters at the 2.5- and 97.5-percent confidence levels after normalizing by the mean for paleoseismic records of Table H1. Upper bound ratios greater than 3:1 are not shown in order to preserve details of the usefully bounded estimates. Blue "x" symbols show parameter ranges using only the closed paleoseismic record. Using the open interval (red "+" symbols) uniformly improves parameter resolution with greatest effects on records with fewer than 6-7 intervals.

Developing Sets of Recurrence Interval Samples

A crucial point in estimates developed in this appendix is that the paleoseismic data at any given site are few in number. At the same time, paleoseismic event dates are, in general, uncertain, and have empirically shaped PDFs. These facts frame the strategy for parameter estimation. Specifically, we sample from the event PDFs to develop possible fault rupture histories, use ML methods to estimate parameters for these histories, and estimate recurrence parameters for the site from ensembles of these individual solutions. The fact that the event dates are uncertain does not increase their number, and dating uncertainty cannot be used as a proxy for process uncertainty.

To sample at random from event PDFs, each PDF is divided into bins narrow on the time axis with their height determined by the probability. We used bins two years wide centered on odd year boundaries. Bins in the central 95 percent of the PDF are divided into 10,000 total small patches of equal probability (their area being two years wide by a probability increment tall). Dates in the middle of the PDF have taller bins and divide into more patches, making those bin years commensurably more likely to be selected. For historical events, all 10,000 patches have

the same date. We have found that the results are generally not sensitive to bin width. An alternate and perhaps more general method would be to vary the bin width inversely to the probability "height" such that 10,000 equal-area slices are produced. A random number generator with uniform probability on 1:10,000 is used to select the sample event date.

Candidate paleoseismic event series are made by drawing from each event PDF independently, then testing the sample series. Earthquake dates commonly overlap in time because of the uncertainties of radiometric dating and evidence preservation. Thus the first test of the event series is one of positivity—that is, within this sample, do the earthquakes occur in the correct order? Series failing this test are discarded and another is drawn. In addition to maintaining independence among resulting interval lengths, this approach implements an ordering-based "shaving" of overlapping event PDFs. Types of sites where this sampling approach can be important include those with flurries of events (for example, Hog Lake, Frazier Mountain, Bidart Fan). An alternative we explicitly avoid is to sample from the events in order of their occurrence. Where event PDFs overlap, this method would create a biased interval sample because a choice from the first PDF could restrict date choices for successive events. Monte Carlo-Markov Chain sampling from events can be used to develop unbiased estimates of parameters such as mean intervals (for example, Oxcal), but we require individual event series to develop ML recurrence interval parameters.

Positivity is a minimum standard for accepting a sample set of recurrence intervals. However, the processes of preservation and identification of paleoseismic events allow an additional constraint to be applied. One constraint in paleoseismic event identification is that resolvable geologic structures must develop between events in order to tell them apart. This means that some amount of time to accumulate sediments can be assumed to separate events. To implement this geologically motivated constraint, a separation of at least fifteen years is assumed, and event series with shorter separations are discarded. This assumption could, in principle, be modified in cases where particular knowledge of the site and events were available. A minimum separation of twenty years was used in Biasi and others (2002) and the A-fault estimates in UCERF2 (Dawson and others, 2008), but the shorter minimum was required to accommodate the historical 1890-1906 interval of the composite northern SAF-Santa Cruz record. Smaller minimum separations typically cause minor increases in σ_{ln}.

Parameter Estimation from Event Series

Each event series is a sequence of exact earthquake dates for which similarly exact interval lengths are computed. For estimates that will use the open interval since the MRE, the final censored interval is computed from the year 2013 unless otherwise noted. In general, left-censor information (earthquake-free time before the oldest event) is not available for California paleoseismic sites, and no use of it was attempted (contrast Parsons, 2008a). For the log-normal recurrence model, the ML estimate of μ_{ln} for each individual event series is the mean of the natural logs of the interval lengths. Standard deviation of the natural logs σ_{ln} is estimated in the same way as the sample variance is computed for Gaussian data, including n-1 in the denominator that makes σ_{ln} an unbiased estimator (Larson, 1982). To estimate the mean log-normal recurrence interval parameters, estimates are compiled for many event series. The mean of the individual estimates of μ_{ln} is adopted as the final estimate.

Confidence intervals for recurrence-interval parameters cannot be taken from the distribution of estimates of μ_{ln}. Consider an historical sequence of events. In that case there is

exactly one mean parameter and no uncertainty in the estimate. Dating uncertainty does lead to a range of estimates of μ_{ln}, but the range says nothing about the actual recurrence-process rate uncertainty. To estimate confidence intervals on the mean μ_{ln}, we can use results for the normal distribution. For an individual sample of recurrence intervals, the range $\pm St(1-\alpha/2)/\sqrt{(n)}$ around the sample mean defines the central $100(1-\alpha)$ percent confidence interval for μ_{ln} (for example, Larson, 1982, p. 385). Here *S* is the sample standard deviation and $t(1-\alpha/2)$ is the argument of the T distribution at which the cumulative *T*-distribution $=1-\alpha/2$. Matlab implements this calculation to estimate confidence intervals of μ_{ln}. Confidence intervals of 2.5, 16, 84, and 97.5 percent are used in UCERF3.

Results

Table H2 gives maximum likelihood estimates and uncertainty ranges for parameters of the log-normal and exponential distributions for paleoseismic sites used to constrain the UCERF3 Grand Inversion. A nominal mean recurrence time can be estimated for a reference point by dividing the number of intervals into the "closed t" column. The oldest paleoseismic event starts the time window. As seen in figure H4, this is an unbiased estimate of the mean recurrence interval length if the open interval is not considered. Inclusion of the open interval increases mean parameters for both the log-normal and exponential distributions. The sometimes radical increase in the exponential recurrence estimate when the open interval is included can be explained by way of the relationship between the exponential and Poisson distributions. If earthquakes are random in time (Poisson), the rate parameter (in units of per year) is the number of earthquakes per total time. If the total time is increased by an open interval, the denominator absorbs this extra time into the revised estimate of the RI. Because the exponential distribution is memoryless, the probability of a future event is unaffected by the wait since the last one. The open time is less influential for the log-normal distribution.

The range of parameter uncertainty is shown as a function of the number of intervals in figure H7. In both plots, uncertainty is shown as a ratio with the mean. The vertical axis has been restricted in both plots to highlight the main trends. Uncertainties for records with only 2-3 intervals can be unstable (table H2). The wider uncertainty range in figure H7 (blue "X" symbols) is for the closed period from the oldest to the youngest event. The inner range (red "+" symbols) shows the uncertainty range when the open interval is used. Two clear trends emerge. First, parameter uncertainty does indeed decrease as the number of intervals increases. There would be cause for concern if this trend were not clear. Second, in most cases using the open interval improves the definition of the mean parameter. The open interval functions in the ML estimator as something like a fractional extra interval. Exceptions to this trend involve sites where the open interval is strongly different from closed event series (for example, Little Salmon) and the use of a time-predictable model might be questioned.

Table H2. Maximum likelihood recurrence model parameters and uncertainties.

[ni, number of interseismic intervals; Closed T, mean estimate time between oldest and youngest event; MRE, years since most recent event; –, not applicable, record is too short; SAF, San Andreas Fault; N. SAF, northern San Andreas Fault; S. SAF, southern San Andreas Fault]

				Lognormal parameters and ranges, including open interval										Exponential parameter and ranges, including open interval				
	ni	Closed T	MRE (yr)	exp(μ)	μ 2.5%	μ 16%	μ 84%	μ 97.5%	σ	σ 2.5	σ 16	σ 84	σ 97.5	λ	λ 2.5	λ 16	λ 84	λ 97.5
Calaveras Fault—North	3	1389	722	511.3	271.2	366.3	705.3	963.8	0.62	0.3	0.41	0.96	1.43	703.7	292.2	454.7	1531.6	3412.3
Compton	5	11110	1209	1629.9	709.3	1067.7	2479.4	3745.6	1	0.67	0.73	1.36	1.84	2463.8	1202.9	1723	4322.7	7588.1
Elsinore—Glen Ivy	5	872	102	161.6	110.1	134	196	237.1	0.45	0.31	0.32	0.6	0.83	194.9	95.1	136.4	342.2	600.1
Elsinore—Julian	1	1503	1755	-	-	-	-	-	-	-	-	-	-	3258.1	883.2	1779.3	18701.8	128688.4
Elsinore—Temecula	2	2012	**	893.1	8.5	471.2	1691.7	94305.8	0.52	0.23	0.35	2.46	16.55	1005.3	361.1	607.1	2804	8306.9
Elsinore—Whittier	1	1397	1801	-	-	-	-	-	-	-	-	-	-	3198.1	867	1746.6	18357.8	126319
Garlock Central (all events)	5	6378	469	882.7	385.5	580.3	1343.8	2020.8	0.98	0.67	0.72	1.34	1.81	1369.5	668.6	958	2403.5	4217.6
Garlock—Western (all events)	4	4729	330	821.1	351	532.2	1260.1	1920.7	0.9	0.6	0.64	1.27	1.77	1264.9	577.1	854.6	2410.9	4642.6
Green Valley—Mason Road	3	605	407	244.8	132.9	179.6	334.1	451.1	0.6	0.22	0.39	0.92	1.4	337.3	140.1	219	737.7	1635.6
Hayward Fault—North	7	2003	300	263.6	170.5	211.9	328.8	407.5	0.61	0.42	0.47	0.8	1.04	329	176.4	240.8	520	818.3
Hayward Fault—South	11	1777	144	151.5	117.1	133	172.7	196.1	0.45	0.33	0.36	0.55	0.68	174.7	104.5	134.9	247.9	349.9
Little Salmon—Strong's Creek	2	2621	10890	3220.4	401.7	1138.2	9240.8	25820.4	1.71	0.3	0.98	2.95	5.07	6755.5	2425	4113.4	18997.7	55782.3
N. SAF—Alder Creek	1	772	106	-	-	-	-	-	-	-	-	-	-	878.1	238	474.2	4984.1	34684.6
N. SAF—Santa Cruz Segment	9	847	106	79.7	48.2	61.6	102.9	131.9	0.8	0.56	0.63	1.02	1.27	105.9	60.5	80	157.1	231.6
N. SAF—Fort Ross	3	924	106	292.9	208.4	245.8	348.8	411.8	0.3	0.19	0.21	0.46	0.67	343.2	142.5	222.7	750.1	1664.3
N. SAF—North Coast	11	2734	106	198.9	128.6	159.1	248.1	307.7	0.75	0.56	0.61	0.93	1.14	258.1	154.4	199.4	366.6	517.1
N. SAF—Offshore Noyo	14	2548	106	162.5	123.3	140.8	186.8	214.1	0.53	0.41	0.45	0.65	0.77	189.5	119.4	150.1	257	346.7
Puente Hills	2	7153	250	3342.7	2219.4	2719.3	4126.4	5034.5	0.3	0.19	0.18	0.49	0.78	3701.8	1328.8	2255.3	10416.1	30566.6
San Gregorio—North	1	525	490	-	-	-	-	-	-	-	-	-	-	1015.3	275.2	554.1	5824.1	40102.5
Rodgers Creek	2	454	304	252.5	107	163.3	393.1	595.9	0.7	0.32	0.41	1.19	1.97	379	136	231.4	1068.6	3129.4
San Jacinto—Hog Lake	13	3237	243	176.4	100.3	132.2	234.8	310.3	1.07	0.78	0.88	1.3	1.57	267.7	166	210.4	367.8	502.8
San Jacinto—Superstition	2	499	462	314.4	93.7	168.7	576.6	1054.9	0.99	0.42	0.58	1.68	2.82	480.5	172.5	290.1	1339.9	3967.2
S. SAF—Carrizo Bidart	5	442	156	89.3	50	66.5	119.9	159.4	0.71	0.4	0.51	0.98	1.34	119.5	58.4	83.6	209.8	368.1
S. SAF—Burro Flats	6	1039	200	159.1	92.7	120.5	209.9	273.2	0.71	0.47	0.54	0.96	1.26	206.6	106.2	148.4	342	562.9
S. SAF—Coachella	6	754	329	131.6	73.1	97.6	177.3	236.9	0.78	0.43	0.58	1.05	1.41	180.5	92.8	129.4	298.3	491.8
S. SAF—Frazier Mountain	7	830	156	104.2	57.4	77.2	141.2	189.2	0.84	0.56	0.64	1.1	1.44	140.8	75.5	103.2	222.9	350.3
S. SAF—Indio	3	660	333	248.4	152.6	193.6	318.2	404.3	0.47	0.22	0.31	0.73	1.1	331	137.5	214.7	723.4	1605.2
S. SAF—Pallett Creek	9	1213	156	120.6	80	98	148.6	182	0.65	0.45	0.51	0.82	1.04	152.1	86.9	114.8	225.6	332.7
S. SAF—Pitman Canyon	6	888	200	140.4	85.9	108.7	180.1	229.5	0.65	0.41	0.49	0.88	1.16	181.4	93.3	129.9	299.4	494.3
S. SAF—Plunge Creek	2	349	200	187.8	110.4	145.5	248.7	319.2	0.43	0.21	0.25	0.72	1.2	274.4	98.5	169.1	780.8	2265.5
S. SAF—Mission Creek, 1000 Palms	4	859	332	231.2	146.9	185	289.6	363.8	0.5	0.26	0.34	0.7	1.03	297.7	135.8	201.5	568.3	1092.6
S. SAF—Wrightwood	14	1333	156	86	61.9	72.7	101.6	119.5	0.65	0.46	0.54	0.78	0.94	106.4	67	84.3	144.4	194.6

* lncluding open intervals

** No open interval available; parameters are for the available closed interval

Table H3. Long-term mean recurrence intervals and rates, and respective uncertainties.

[Lat, latitude of site; Long, longitude of site; N_{events}, number of events in time T; T, time between the oldest and youngest events; MRE, most recent event; MRI, mean recurrence interval; yr, years; %, percent; S. SAF, southern San Andreas Fault; N. SAF, northern San Andreas Fault]

Site	Lat	Long	N_{events}	T closed	T since MRE	Long-term MRI (yr)	2.5%	16%	84%	97.5%	Mean long-term rate	2.5%	16%	84%	97.5%
Calaveras Fault—North	37.5104	-121.8346	4	1375	720	618.1	321.3	446.1	858.8	1189.1	0.001618	0.000841	0.0011644	0.0022419	0.0031128
Compton	33.9660	-118.2629	6	11102	1207	2658.4	1163.8	1748.1	4059.3	6072.3	0.0003762	0.0001647	0.0002464	0.0005721	0.0008592
Elsinore—Glen Ivy	33.7701	-117.4909	6	874	102	179.1	122.3	147.7	216	262.3	0.0055828	0.0038119	0.0046288	0.00677	0.0081764
Elsinore—Julian	33.2071	-116.7273	2	1502	1753	3251.1	881.3	1779.3	18701.8	128410.1	0.0003076	0.0000078	0.0000535	0.000562	0.0011347
Elsinore—Temecula	33.4100	-117.0400	3	2011	N/A	1019.2	11	533.1	1914	94145.3	0.0009812	0.0000106	0.0005225	0.0018758	0.090633
Elsinore—Whittier	33.9303	-117.8437	2	1400	1799	3197	866.7	1746.6	18357.8	126276.6	0.0003128	0.0000079	0.0000545	0.0005725	0.0011538
Garlock Central (all events)	35.4441	-117.6815	6	6379	471	1435	625.5	940.6	2178.1	3292.3	0.0006969	0.0003037	0.0004591	0.0010631	0.0015988
Garlock—Western (all events)	34.9868	-118.5080	5	4716	330	1230.2	523.5	797.8	1889	2890.7	0.0008129	0.0003459	0.0005294	0.0012535	0.00191
Green Valley—Mason Road	38.2341	-122.1619	4	606	406	293.3	158.7	214.7	399.4	542.1	0.0034094	0.0018448	0.0025038	0.004657	0.0063008
Hayward Fault—North	37.9306	-122.2977	8	2003	300	318.3	205.8	255.3	396.2	492.4	0.0031413	0.0020308	0.0025239	0.0039174	0.0048591
Hayward Fault—South	37.5563	-121.9739	12	1778	144	167.6	129.4	147	190.8	217	0.0059677	0.0046073	0.0052416	0.0068047	0.0077298
Little Salmon—Strong's Creek	40.6002	-124.1218	3	2625	10877	6750.8	2423.3	4113.4	18997.7	55743.8	0.0001481	0.0000179	0.0000526	0.0002431	0.0004127
N. SAF—Alder Creek	38.9813	-123.6770	2	764	106	869.7	235.8	474.2	4984.1	34349.9	0.0011499	0.0000291	0.0002006	0.0021088	0.0042417
N. SAF—Santa Cruz Seg.	36.9626	-121.6981	10	848	106	109.8	66.3	85	142	182.1	0.0091041	0.0054923	0.0070415	0.0117617	0.0150912
N. SAF—Fort Ross	38.5200	-123.2400	4	922	106	306.3	217.8	257.6	365.5	430.7	0.003265	0.0023217	0.0027356	0.0038814	0.0045915
N. SAF—North Coast	38.0320	-122.7891	12	2732	106	263.9	170.4	211.4	329.6	408.5	0.0037898	0.0024481	0.0030343	0.0047303	0.0058668
N. SAF—Offshore Noyo	39.5167	-124.3333	15	2548	106	187.6	142.1	162.8	216	247.8	0.0053293	0.004035	0.0046304	0.0061415	0.0070387
Puente Hills	33.9053	-118.1104	3	7167	251	3505.9	2346.4	2842.2	4312.8	5238.3	0.0002852	0.0001909	0.0002319	0.0003518	0.0004262
San Gregorio—North	37.5207	-122.5135	2	530	484	1019.1	276.3	554.1	5824.1	40250.5	0.0009813	0.0000248	0.0001717	0.0018047	0.0036199
Rodgers Creek	38.2623	-122.5334	3	454	303	325.3	134.8	208.8	502.7	785	0.003074	0.001274	0.0019892	0.004789	0.0074173
San Jacinto—Hog Lake	33.6153	-116.7091	14	3236	243	311.8	176.9	233.9	415.5	549.4	0.0032074	0.0018202	0.0024066	0.0042752	0.0056519
San Jacinto—Superstition	32.9975	-115.9436	3	503	462	508.3	153.2	274.3	937.5	1686.6	0.0019675	0.0005929	0.0010666	0.0036454	0.0065288
S. SAF—Carrizo Bidart	35.2343	-119.7887	6	441	156	114.7	64.1	85.5	154.1	205.1	0.0087179	0.0048746	0.0064913	0.0117016	0.0155916
S. SAF—Burro Flats	33.9730	-116.8170	7	1040	200	205.4	119.2	156.1	271.7	354.1	0.0048677	0.002824	0.0036799	0.0064073	0.0083903
S. SAF—Coachella	33.7274	-116.1701	7	753	329	178.5	99.2	132.4	240.6	321.1	0.0056037	0.0031142	0.0041571	0.0075507	0.0100834
S. SAF—Frazier Mountain	34.8122	-118.9034	8	829	156	148.6	81.9	110	201.2	269.4	0.0067307	0.0037115	0.0049697	0.0090886	0.0122057
S. SAF—Indio	33.7414	-116.1870	4	659	334	277.4	171.5	216.9	356.5	448.7	0.0036053	0.0022287	0.002805	0.0046111	0.0058323
S. SAF—Pallett Creek	34.4556	-117.8870	10	1213	156	149.3	98.9	121.1	183.6	225.3	0.006698	0.0044376	0.005447	0.0082553	0.0101097
S. SAF—Pitman Canyon	34.2544	-117.4340	7	887	200	173.5	105.8	134.9	223.5	284.5	0.0057643	0.003515	0.0044747	0.0074149	0.0094529
S. SAF—Plunge Creek	34.1158	-117.1370	3	350	200	205.4	122.2	159.3	272.3	345.2	0.0048695	0.0028965	0.0036725	0.0062762	0.0081864
S. SAF Mission Creek—1,000 Palms	33.8200	-116.3010	5	859	330	261.3	166.8	208.4	326.1	409.4	0.0038266	0.0024425	0.0030666	0.0047993	0.0059951
S. SAF—Wrightwood	34.3697	-117.6680	15	1335	156	106	76.2	89.7	125.4	147.5	0.0094304	0.0067778	0.0079741	0.0111519	0.0131212

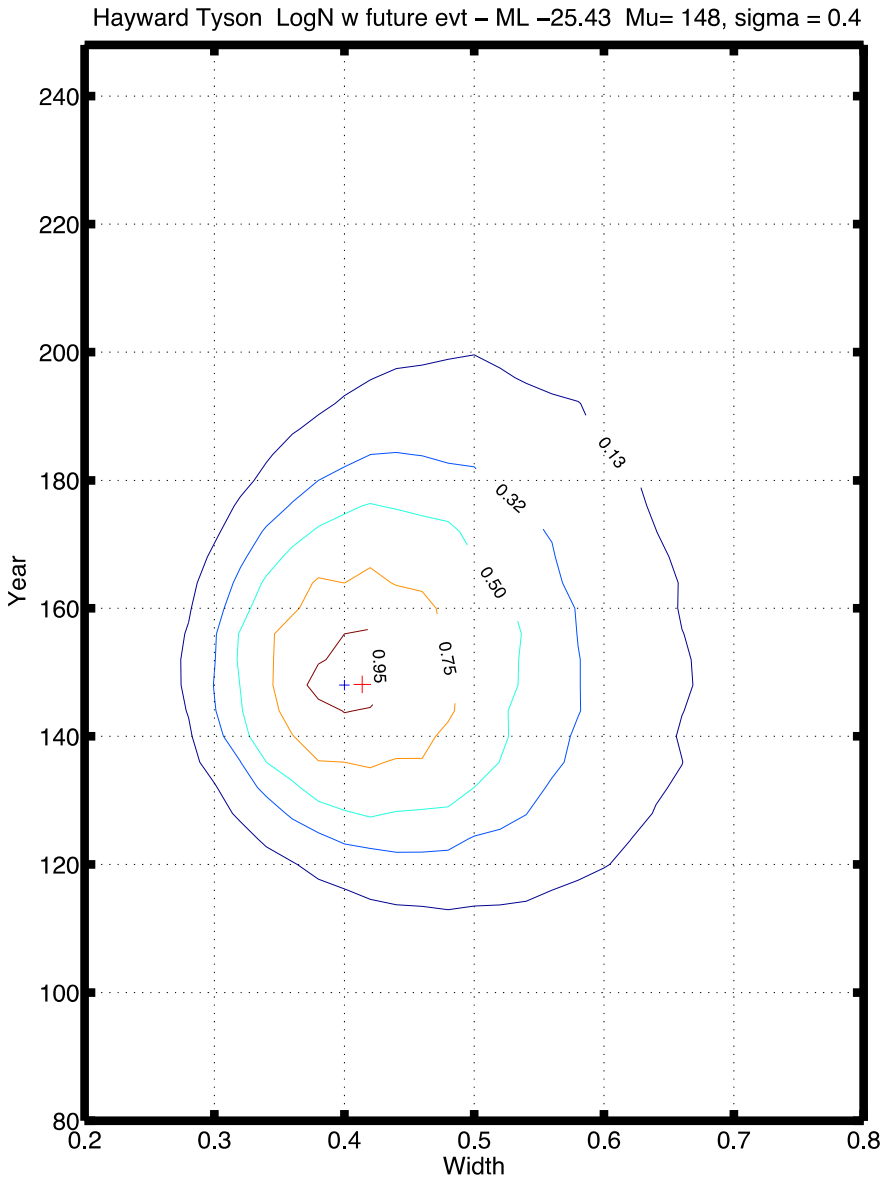

Figure H7. Plot showing the log-normal likelihood surface for the southern Hayward fault site at Tyson's Lagoon (Lienkaemper and others, 2010). This site shows a well-resolved maximum at μ_{ln}=148, σ_{ln}=0.40. The maximum differs slightly from table H2 (151.7, 0.45) because of slight differences in handling the open interval and run-to-run differences that arise, because both are based on random sampling from the date probability distribution functions. The 0.32 contour corresponds to the central 68-percent probability region for this appendix. Uncertainties in table H2 (133≤ μ_{ln} ≤ 173, 0.36≤σ_{ln} ≤ 0.55) are similar but slightly narrower than the extrema of the 0.32 contour. Neither μ_{ln} or σ_{ln} can be fully expressed as a range because they trade off at equal likelihood levels. The contour levels correspond to real probabilities, so the likelihood of alternative parameter estimates can be read directly. For example, the UCERF2 estimate of 210 years for the 11-event Hayward record (Parsons, 2008b) would now seem unlikely.

Maximum likelihood estimates and ranges can be visualized and specific estimates may be quantitatively compared by plotting a likelihood surface (fig. H8; Biasi and Scharer, 2012). Each point on this plot is associated with some pair of μ,σ of a log-normal model. To estimate the relative likelihood of any individual paleoseismic sequence, a probability of each individual interval length is calculated. To relate the continuous log-normal distribution to discrete outcomes, the log-normal distribution is binned in 2-year widths, so the probability of the interval, numerically, is actually the probability that it falls in a two-year window. Parametric results do not depend materially on the discretization. The likelihood function for a given μ,σ is the product of the individual probabilities across all intervals. On contouring, the ML parameters μ_{ln}, σ_{ln} are selected from the peak. A water-level approach is taken to develop confidence contours in which, starting from the peak, the level is progressively lowered until it encloses some level of total probability. Figure H8 shows an example for the Southern Hayward fault paleoseismic site. The maximum value of this surface is at μ_{ln}=148, σ_{ln}=0.40, and quite close to the values in table H2. The contour levels may be interpreted as parameter pairs, which could explain the data with equal probability. They also show that the parameters at any given likelihood level are not independent of one another.

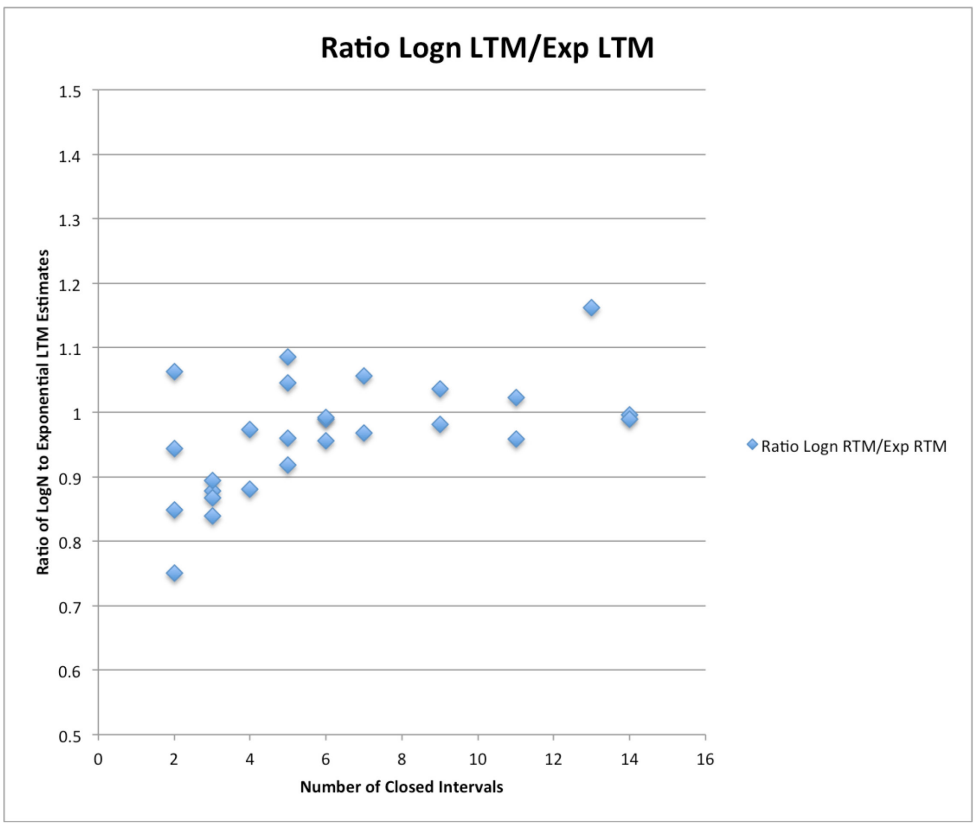

Figure H8. Ratio of long-term log-normal mean recurrence interval estimates to exponential model estimates for paleoseismic sites with three or more earthquake dates. For paleoseismic records with five or more intervals, the estimates are within 10 percent of each other. The declining ratio for some sites with 4 or fewer intervals is due to the strong effect of the open interval length on exponential estimates.

The likelihood plots can be used to check how important the event date PDF structure is for parameter estimation. To do this we replace the dating structure from Bayesian analysis of the radiocarbon dates with uniform PDFs on their 95-percent date ranges. Figure H9 shows the results. Compared to figure H8, the main effect of neglecting the dating structure is to increase the σ_{ln} estimate and its uncertainty. Parsons (2008b) also estimated recurrence for the Southern Hayward site with a method that neglects event date structure. Figure H9 indicates that the UCERF2 recurrence interval estimate of 210 years is would be improbable by a factor of 20 to 100 compared to the maximum likelihood estimate. Part of the difference might be explained by the current event series now including one more earthquake than the UCERF2 estimate (Lienkaemper and others, 2010), but other causes are apparently also at work.

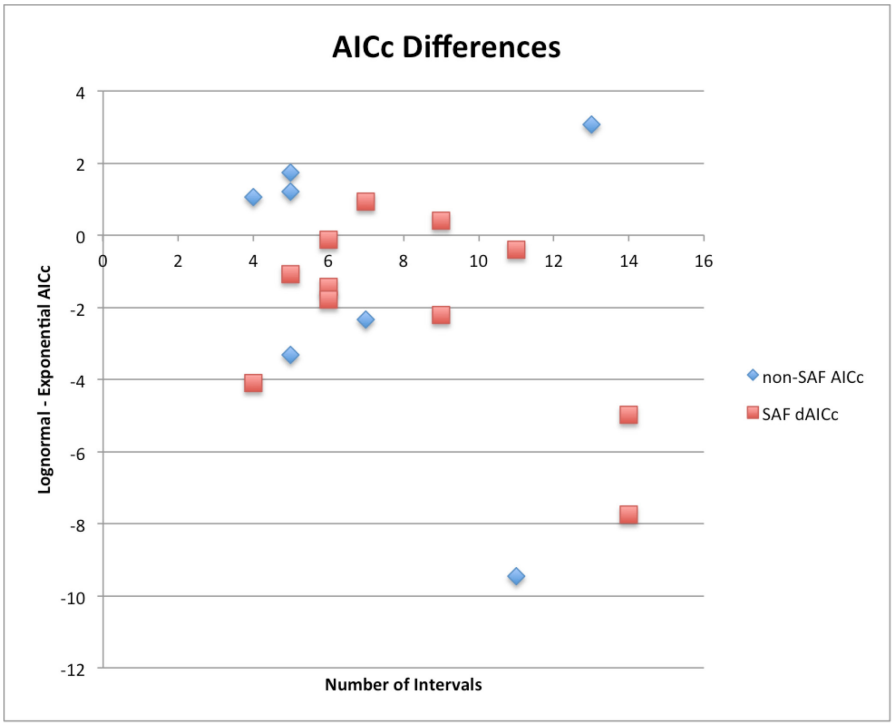

Figure H9. Plot showing the differences of modified Akaike Information Criteria (AICc) between the log-normal and exponential models. Negative differences correspond to cases where the log-normal model fits the data better than the exponential even after correcting for the additional parameters. The AICc also adjusts for the small sample size. San Andreas Fault sites (red squares) and non-San Andreas sites (blue diamonds) are separated to explore whether the log-normal model cases concentrate in mature faults. These data may show some site-averaged preference for the log-normal model, but at least show that the log-normal distribution is not an unreasonable basis for estimating the time-independent long-term mean recurrence parameters.

Because both the exponential and log-normal models give long-term mean (LTM) recurrence intervals and rates, the question becomes which distribution should be used to provide the estimates. Figure H10 shows the difference between these estimates as a ratio of the log-normal to exponential LTM.

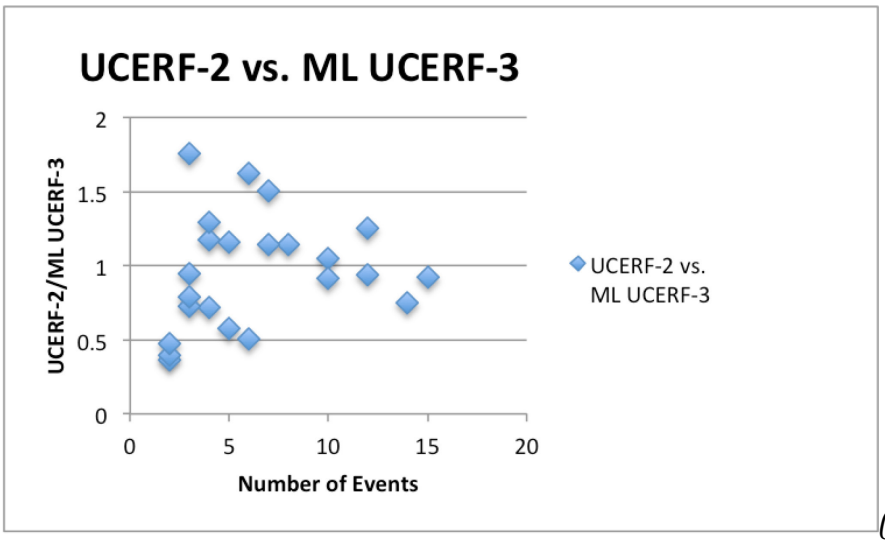

(A)

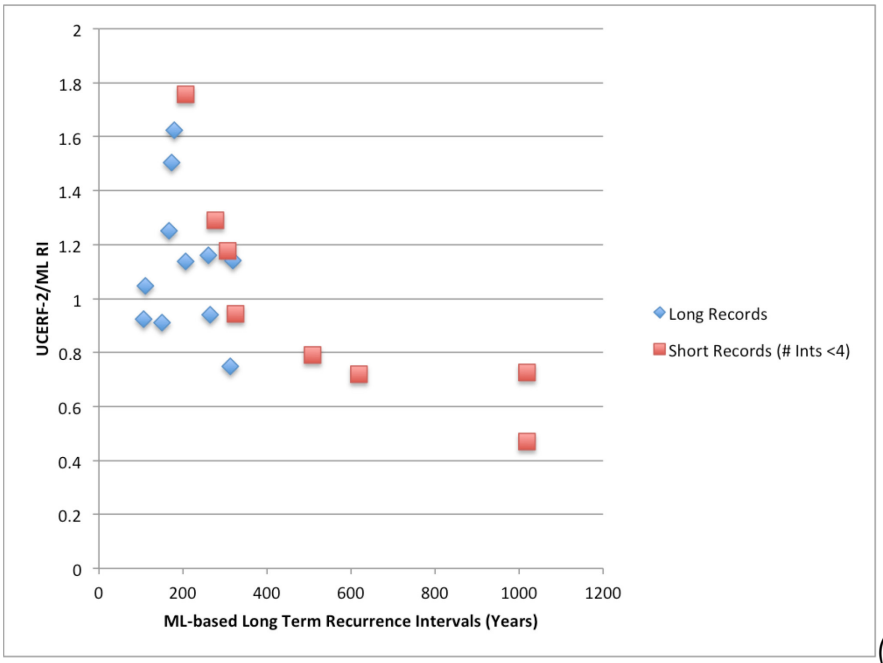

(B)

Figure H10. Plots comparing of recurrence interval between UCERF2 and the present maximum likelihood-based estimates. *A,* UCERF2 recurrence-rate estimates compared with maximum likelihood long-term means. UCERF2 estimates differ in how they were calculated and do not formally include the open intervals since most recent events. *B,* A systematic relationship is observed between the UCERF2 recurrence-interval (RI) estimates made from short paleoseismic records and their corresponding maximum likelihood-based values. The difference is primarily due to how the open intervals were incorporated. Two long- and two short-record points with RI>1,200 years are not shown to preserve visibility of the most active faults. They follow the descending trend of the data shown.

Maximum likelihood parameter estimates for both models are asymptotically unbiased, so as may be seen, long-term mean interval estimates from the two distributions converge for long

records. For short records the two estimates can differ, primarily because of how they integrate the open interval since the MRE. The exponential distribution estimate is based on the total time with event coverage divided by the number of intervals in that time. The LTM thus increases by T/n-intervals for T=time since the MRE. For example, for a record of two intervals with a closed average of A and T~A, the exponential LTM estimate increases by about 1/3. If the event happens at T=A, the parameter estimate would immediately revert to A. The log-normal distribution is much less sensitive to the length of the open interval. The predicted divergence of LTM estimates for short records and their similarities for long ones are evident in figure H10. If we view the time since the MRE as an accident of the sample, figure H10 suggests that the log-normal estimates will tend to be more robust.

We explore an alternative model comparison method using the modified Akaike Information Criteria (AICc*;* Hurvich and Tsai, 1989; Burnham and Anderson, 2002). The original definition of the Akaike Information Criteria (AIC; Akaike, 1974) is a measure of model fit used to compare models at their maximum likelihood points, $\mathcal{L}(\theta|g)$, after compensating for differences in the number of parameters K in the model g:

$$\mathrm{AIC} = -2*\log(\mathcal{L}(\theta|g)) + 2K \qquad (5)$$

The AICc measure adjusts the AIC in equation 5 to compensate for cases where the sample size is not large with respect to the number of data, n:

$$AICc = AIC + \frac{2K(K+1)}{n-K-1} \qquad (6)$$

As may be seen in equation 6, the AICc criteria is not defined for the log-normal model for fewer than n=4 sample recurrence intervals. Figure H11 shows the difference in AICc estimates between the exponential and log-normal models. For sample sizes of 7 or more the AIC and AICc are very similar. AICc differences of two can be considered good support for one model over another. The data slightly favor the log-normal recurrence model, even after compensating for the additional model parameter of the log-normal model. This is consistent with findings by others that most long paleoseismic records in California exhibit at least some degree of time predictability (Biasi and others, 2012; Parsons, 2008b; Scharer and others, 2010). However this debate is resolved in the future, and whether better measures than the AICc may be proposed in future model comparisons, the clear message in figure H11 is that the log-normal model shape is at least a reasonable choice for estimating long-term mean recurrence intervals and rates.

Long-term mean recurrence intervals are calculated using equation 3 and given in table H3. Long-term mean recurrence rates are obtained from the intervals by a simple reciprocal. For records of three or fewer events, the log-normal parameters are not resolved, and exponential parameters and uncertainties are given instead. An exception was made for the Little Salmon site, where the event series consists of three events in a 2,500-year period ending about 9,000 B.C.E., then an 11,000-year hiatus. The time since the MRE effectively contradicts the log-normal model from the two definite intervals, and so inflates σ_{ln} that the equation 3 long-term-mean interval made no sense. As a result, the exponential parameters are given in table H3 for the Little Salmon site. In a review of the original report for the site (Hemphill-Haley and Witter,

2006), investigators indicated that they considered it likely that their event record reflected temporal clustering on a fault splay and that it was not characteristic of the fault as a whole. As a result we recommend that this site not be used to constrain the Grand Inversion.

ML-based long-term mean rate estimates can be compared with estimates for UCERF2 (fig. H12; Dawson and others, 2008; Parsons, 2008a). UCERF2 RI estimates are generally distributed around the current ML values (fig. H12*A*), but with significant scatter. In figure H12*B* ratios of UCERF2 to ML mean recurrence interval are plotted versus the RI itself. This view provides a way of separating the UCERF2 estimates, which were based on an ML-informed approach and the BPT model (Parsons, 2008a). Since the BPT location parameter is approximately the long-term mean, differences should not be due to model parameterization.

Discussion

Use of maximum likelihood methods for recurrence-interval parameter estimation is not new. Biasi and others (2002) applied them to the Wrightwood and Pallett Creek records. Parsons (2008a) used an implicit maximum likelihood method to estimate recurrence parameters using exponential and BPT models. In that study the likelihood basis was implemented by trying ten million random samples per μ, σ pair over a large range of candidate parameters. The origin of differences between that method, also used for UCERF2, and the present estimates, is unclear. Parsons (2008a) neglects event dating structure within event series, replacing event-date PDFs with uniform distributions. A more important potential source could be unintended consequences of an extra interval apparently inserted before the oldest event in order to give the sampling method a definite starting point. Biasi and Scharer (2012) found RI parameter estimates lengthened, especially for short series, when an analogous unbounded future event was included with the current open interval. Something of this nature is suggested by figure H12*B*. In all, however, our attempts to reproduce the bias in ML estimates reported by Parsons (2008a) have thus far been unsuccessful.

Tests for bias in log-normal parameter estimates (figs. H4 and H5) make two points important for understanding their use in rupture rate estimates. First, when a set of intervals is drawn from a true log-normal process and analyzed as a closed total interval bounded by earthquakes, on average there is no bias in ML estimates of the parameters. Individual samples may vary according, of course, but in ways consistent with uncertainty in the fitting parameters. Second, when data are analyzed like most paleoseismic event series, adopting as a time window the oldest event to the present day, a bias is introduced, but it is modest in magnitude and readily explained. This approach neglects the open interval before the oldest event. The expected time thus neglected is about half a recurrence interval. For the log-normal model, this part of the censored interval contains the least information about parameter values. What effect it does have on μ_{ln} is then reduced by the number of intervals. This leads to the stability in long-term mean intervals discussed in association with figure H10. For representative California fault recurrence rates (fig. H5), parameter bias from this approach is expected to be a few percent or less.

Future studies might give closer examination to the fitness of the log-normal model relative to other candidates, including the Brownian Passage Time and Weibull distributions. The log-normal model has the unattractive quality that the hazard function begins to decline after the mean recurrence time and asymptotically approaches zero when the open interval since the MRE is very long compared to the average recurrence interval (Matthews and others, 2002). However, with the apparent exception of the Little Salmon site, times since the MRE for California's

paleoseismic records are similar to the RIs, meaning that the log-normal model will provide a reasonable approximation of the time-dependent hazard at those sites.

We have not attempted to resolve the relative merits of a time-dependent model relative to the less prescriptive exponential distribution. It is true that small samples of recurrence intervals from a random process can sometimes appear regular, but short samples of a modestly time-dependent model can also appear random. Dating uncertainty makes conclusions from short series that much more difficult. For short series one might argue that the data do not justify two fitting parameters, but neither can they offer a positive argument for using only one. Tests with the AICc tend to confirm this conclusion (fig. H11). However, if we instead focus on the longest records, most sites exhibit a coefficient of variation (COV) of 0.5 to 0.8, compared to a COV near 1.0 for truly random processes (Biasi and others, 2012). This comprises positive evidence for time dependence, but leaves to speculation whether the shorter records of the present data set would follow this pattern.

The fact that the Grand Inversion uses the long-term rate without reference to the internal structure of the earthquake sequence reduces the impact of not being able to resolve a best recurrence model. For long records we find that mean recurrence intervals from exponential and log-normal long-term means are very similar, so that compared to other sources of uncertainty, the marginal impact of the choice of models is small. Our use of equation 3 and the log-normal model has been preferred here because it makes consistent use of estimators both for the long-term means and time dependence at most individual sites. In addition, as seen in figure H10, the long-term means from the log-normal model tend to be less dependent on the time since the MRE. This is as it should be for long-term estimates.

It has been pointed out that if the log-normal model is correct, most recurrence intervals will be shorter than the long-term mean, and the actual hazard may be higher than inferred from the long-term mean. This is an unavoidable consequence of using a time-independent method to estimate rupture recurrence. Hazard is outside the scope of this appendix, but we can at least note here that the paleoseismic data provide encouragement to pursue the long-term time-dependent component of hazard estimation both within UCERF3 and in future research.

References

Akaike, H., 1974, A new look at the statistical model identification: IEEE Transactions on Automatic Control, v. 19, no. 6, p. 716–723.

Burnham, K.P., and Anderson, D.R., 2002, Model selection and multi-model inference— A practical information theoretic approach: New York, Springer, p. 488.

Bakun, W.H., and Lindh, H.G., 1985, The Parkfield, California earthquake prediction experiment: Science, v. 229, no. 4714, p. 619–624.

Biasi, G.P. and Scharer, K.M., 2012, A new likelihood method for estimating recurrence interval parameters from paleoseismic event series: Seismological Research Letters, v. 83, p. 441.

Biasi, G.P., Berryman, K.R., Cochran, U.A., Clark, K., Langridge, R.M., and Villamor, P., 2012, Earthquake recurrence on continental transform faults—Alpine fault, New Zealand and San Andreas fault, California compared [abs.]: Eos (Transactions of the American Geophysical Union), v. 93, Fall meeting supplement, abs. S51F–06.

Biasi, G.P., Weldon, R.J., Fumal, T.E., and Seitz, G.G., 2002, Paleoseismic event dating and the conditional probability of large earthquakes on the southern San Andreas fault, California: Bulletin of the Seismological Society of America, v. 92, p. 2761–2781.

Biasi, G.P. and Weldon, R.J., II, 1994, Quantitative refinement of calibrated C-14 distributions: Quaternary Research, v. 41, p. 1–18.

Cornell, C.A., and Winterstein, S.R., 1988, Temporal and magnitude dependence in earthquake recurrence models: Bulletin of the Seismological Society of America, v. 78, p. 1522–1537.

Dawson, T.E., Weldon, R.J., and Biasi G.P., 2008, Appendix B—Recurrence interval and event age data for type A faults: U.S. Geological Survey Open-File Report 2007–1437–B, 38 p., *http://pubs.usgs.gov/of/2007/1437/b/*.

Ellsworth, W.L., Matthews, M.V., Nadeau, R.M., Nishenko, S.P., Reasenberg, P.A., and Simpson R.W., 1999, A physically-based earthquake recurrence model for estimation of long-term probabilities: U.S. Geological Survey Open-File Report 99–520, 22 p., *http://geopubs.wr.usgs.gov/open-file/of99-522/*.

Field, E.H., Dawson, T.E., Felzer, K.R., Frankel, A.D., Gupta, V., Jordan, T.H., Parsons, T., Peterson, M.D., Stein, R.S., Weldon, R.J., II, and Wills, C.J., 2009, Uniform California earthquake rupture forecast—version 2 (UCERF2): Bulletin of the Seismological Society of America, v. 99, p. 2053–2107, doi:10.1785/0120080049.

Fisher, R.A., 1922, On the mathematical foundations of theoretical statistics: Philosophical Transactions of the Royal Society of London, Series A, v. 222, p. 309–368.

Hemphill-Haley, M.A., and Witter, R.C., 2006, Latest Pleistocene paleoseismology of the southern Little Salmon fault, Strong's Creek, Fortuna, California: Final Technical Report, NEHRP Award #04HQGR004, *http://earthquake.usgs.gov/research/external/reports/04HQGR0004.pdf*, p. 19.

Hurvich, C.M. and Tsai C.L., 1989, Regression and time series model selection in small samples: Biometrika, v. 76, p. 297–307.

Larson, H.J., 1982, Introduction to probability theory and statistical inference: New York, John Wiley and Sons, 637 p.

Lienkaemper, J.J., Williams, P.L., and Guilderson, T.P., 2010, Evidence for a twelfth large earthquake on the southern Hayward fault in the past 1900 years: Bulletin of the Seismological Society of America, v. 100, p. 2024–2034, doi:10.1785/0120090129.

Lienkaemper, J. J. and Bronk, C.B., 2009, OxCal—A versatile tool for developing paleoearthquake chronologies—a primer: Seismological Research Letters, v. 80, p. 431–434.

Matthews, M.V., Ellsworth, W.L., and Reasenberg, P.A., 2002, A Brownian model for recurrent earthquakes: Bulletin of the Seismological Society of America, v. 92, p. 2233–2250.

Parsons, T., 2012, Paleoseismic interevent times interpreted for an unsegmented earthquake rupture forecast: Geophysical Research Letters, v. 39, L13302, doi:10.1029/2012GL052275.

Parsons, T., 2008a, Monte Carlo method for determining earthquake recurrence parameters from short paleoseismic catalogs—Example calculations for California: Journal of Geophysical Research, v. 113, V03302, doi:10.1029/2007JB004998.

Parsons, T., 2008b, Earthquake recurrence on the south Hayward fault is most consistent with a time dependent renewal process: Geophysical Research Letters, v. 35, L21301, doi:10.1029/2008GL035887.

Savage, J.C., 1993, The Parkfield prediction fallacy: Bulletin of the Seismological Society of America, v. 83, p. 1–6.

Scharer, K.M., Biasi, G.P., and Weldon, R.J., II, 2011, A reevaluation of the Pallett Creek earthquake chronology based on new AMS radiocarbon dates—San Andreas fault, California: Journal of Geophysical Research, v. 116, B12111, doi:10.1029/2010JB008099.

Scharer, K.M., Biasi, G.P., Weldon, R.J., and Fumal, T.E., 2010, Quasi-periodic recurrence of large earthquakes on the southern San Andreas fault: Geology, v. 38, no. 6, p. 555–558, doi:10.1130/G30746.1.

Sykes, L., and Menke, W., 2006, Large earthquakes—Implications for earthquake mechanics and long-term prediction: Bulletin of the Seismological Society of America, v. 96, p. 1569–1596, doi:10.1785/0120050083.